2023 IEEE/ASME International Conference on Advanced Intelligent Mechatronics (AIM)
June 28-30, 2023. Seattle, Washington, USA

Null-Space-Based Adaptive Control for Aerial Manipulators on Cooperatively Transporting Cable-Suspended Objects

Te-Kang Hung, Yen-Chen Liu, and Chen-En Lee

***Abstract*—This paper proposes a system framework for aerial manipulators to cooperatively transport a cable-suspended load. If the trajectory of the payload is considered as the control object, the entire system of the aerial manipulators and the slung load is redundant. Therefore, the null-space-based (NSB) controller can be presented to ensure the position/orientation of the slung load via the control for the quadrotors and robotic arm. The load trajectory and interactive force on the aerial manipulator during transportation are investigated. Additionally, the adaptive control method is presented in the inner controller to keep the control performance under dynamic uncertainties, interactive forces, and unknown load. To demonstrate the stability and efficacy of the proposed control structure, Lyapunov stability analysis, and numerical simulations are presented.**

***Keywords*—Adaptive control, null-space-based control, aerial manipulation, obstacle avoidance, cooperative transportation**

I. Introduction

Multirotors are a type of unmanned aerial vehicles (UAVs), that have attracted tremendous attention in recent years resulting from extensive applications. Such systems are convenient for features such as vertical take-off and landing (VTOL), simple structure, and tailored capabilities [1]–[3]. The advantageous agility and mobility of UAVs contribute to their application in several domains, including transportation, surveillance, and structure inspection [4]–[6]. Moreover, to enhance the features of UAVs and realize aerial manipulation platforms in practice, various types of tools are added with suitable control strategies. Such strategies include intelligent control methods, adaptive control, and other control strategies as proposed in [1], [7], [8].

Recently, the topic of aerial manipulators, which are a combination of robotic arms and UAVs, has become an emerging research direction in robotic and mechatronic societies [5], [7], [9]. Such mechatronic systems can make the UAVs significantly maximize the mobile manipulation utility. To handle or interact with objects in practical applications, cables, grippers, and manipulators have been installed on the bases of the quadrotors [5], [10], [11]. Lifting and transporting the load by using the linear quadratic regulator (LQR) was proposed in [10]. In [11], an aircraft system equipped with a cable-driven gripper was proposed with the designed control method for the maneuvering control of the system. The DDPG-based reinforcement learning approach was presented in the decoupling aerial manipulator system to ensure the effectiveness of the manipulator motion to quadrotor [5]. To enhance the capability and mobility of multi-UAV transportation, the latest research was proposed in [9], [12]–[14]. Control barrier functions were used for two UAVs to collaboratively move a payload to a target location around obstacles in [12]. In [13], using cable-suspended payload multi-UAVs system, MAVs equipped with monocular vision and inertial sensing were used to address the trajectory tracking, state estimation, and control method.

Cooperative aerial transportation can have better-carrying performance compared to single UAVs with bulkier and heavier loads. In [15], a team of UAVs grasps an object through a single contact point at the tooltip and transport an object based on compliant force control. The aerial manipulator cooperative transportation with impedance control to restrict the contact force was given in [16]. However, the controller was designed based on the measurement of force/torque at the wrist by the end-effectors, which impedes the system from being implement in practice. The aerial cooperation with one UAV as a leader and other UAVs as followers was implemented in [17], [18]. However, such approaches are subject to a single point of failure since the system relies on the master agent as the central unit for navigation.

The dynamic model of the dual aerial manipulator cooperative transportation system is highly coupled and composed of the UAV, manipulator, and load. Therefore, the interactive forces between the motion of UAVs and manipulators should be carefully considered in the controller design. If the interactive forces between the aerial manipulator and load are not well resolved, the stability of the system would significantly degrade and make the system dangerous. Therefore, an aerial manipulator controller should be able to tolerate the interactive forces for each part of the cooperative aerial transportation system. Several unforeseen problems in cooperative aerial transportation systems may cause aerial robots to lose tracking performance or even lose stability as a result of factors such as disturbances, interactive force, and unknown parameters.

In this paper, we propose a novel null-space-based controller to achieve cooperative aerial transportation for a slung load. To achieve these goals, we concentrate on three parts: 1) load for leader-based tracking 2) behavioral coordinated control for the aerial manipulation 3) adaptive controller design for the aerial manipulators. In the proposed system, only need to give the desired trajectory of the load as the leader, and the aerial manipulator may track the desired trajectory consensus from each agent. Moreover, the proposed controller can keep the load-tracking performance when the UAV is close to the obstacle.

The rest of this paper is organized as follows. A brief

This work was supported by the National Science and Technology Council (NSTC), Taiwan, under Grant NSTC 112-2636-E-006-001.

T.-K. Hung, Y.-C. Liu and C.-E Lee are with the Department of Mechanical Engineering, National Cheng Kung University, Tainan 70101, Taiwan. E-mail: {n16100200@ncku.edu.tw, yliu@mail.ncku.edu.tw, n16101727@ncku.edu.tw}.

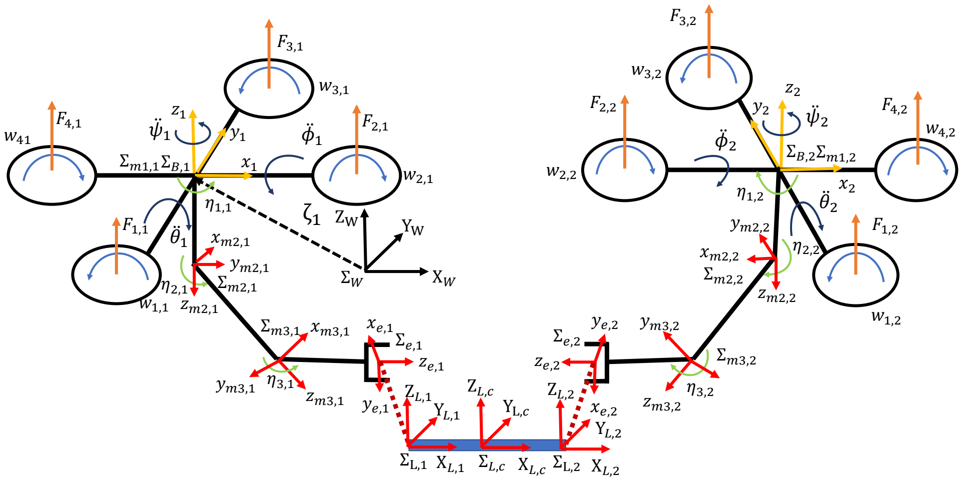

Fig. 1: Sketch and coordinates of the dual aerial manipulator with a slung load.

background in modeling the quadrotor dynamics and the manipulator dynamic is shown in Section II. In Section III, the force analysis and trajectory design are presented for the slung load cooperatively transported by the aerial manipulators. The controller design and stability analysis for the system are addressed in Section IV. The simulation examples of the proposed dual aerial manipulator transportation with cable-supported are validated in Section V. The conclusion and future work of this paper are summarized in Section VI.

II. Preliminaries and System Modeling of Aerial Manipulator

The proposed cooperative transportation system is composed of two aerial manipulators with a slung load connected to the end-effectors. The entire system is illustrated in Fig. 1, where each quadrotor is mounted with a three-DOF manipulator with revolute joints. The payload is tied steadily via suspended cable to the gripper of the manipulators. The kinematic and dynamic modelings of the aerial manipulator are addressed in this section. Since the design and configuration of the aerial manipulators are identical, the following derivation is stated for the generalized form. In the following sections, the subscript $i = \{1, 2\}$ will be considered to denote the two aerial manipulators as shown in Fig. 1.

We consider $\zeta = [x, y, z]^T \in \mathbb{R}^3$ and $\Phi = [\phi, \theta, \psi]^T \in \mathbb{R}^3$ as the position and orientation of the quadrotor frame Σ_B with respect to the world frame Σ_w. From the based frame of the quadrotor Σ_B, the joint angles of the manipulators and task-space position at the end-effector are given as $\eta = [\eta_1, \eta_2, \eta_3]^T \in \mathbb{R}^3$ and $X_e = [x_e, y_e, z_e]^T \in \mathbb{R}^3$, respectively. The first joint of the manipulator rotates with respect to the z-axis of Σ_B, and the subsequent two joints rotate along the y-axis of Σ_B. For the robotic manipulator, $\Sigma_{mj}, j = \{1, 2, 3\}$ are denoted as the coordinate of each joint, and Σ_e is the end-effector frame. The coordinate frames of the connecting point on the load to the cable are denoted by Σ_L, and $\Sigma_{L,c}$ is the center of mass of the slung load.

The generalized coordinates of the quadrotor with a manipulator are considered as $q = [\zeta^T, \Phi^T, \eta^T]^T \in \mathbb{R}^9$, where $\Phi = [\phi, \theta, \psi]^T \in \mathbb{R}^3$ is the Euler angles of each quadrotor, and $\eta = [\eta_1, \eta_2, \eta_3]^T \in \mathbb{R}^3$ is the joint angle of each manipulator. The velocity between the world coordinate Σ_w to the body frame Σ_B is given as $\dot{\zeta} = \mathbf{R}V_B$ and $\Omega_i = \mathbf{T}\omega_B$, where $V_B, \omega_B \in \mathbb{R}^3$ are the linear and the angular velocities in Σ_B, respectively, Ω is the Euler angle of the quadrotor in Σ_W, $R \in \mathbb{R}^{3\times3}$ is the rotation matrix, and $T \in \mathbb{R}^{3x3}$ is the translation matrix. The rotation matrix $R \in SO(3)$ is obtained from Σ_B to Σ_W with the use of z-y-x Euler angles. Thus, the matrices R and T are given as

$$\mathbf{R} = \begin{bmatrix} c_\psi c_\theta & -s_\psi c_\phi + c_\psi s_\theta s_\phi & c_\psi s_\theta c_\phi + s_\psi s_\phi \\ c_\theta s_\psi & c_\phi c_\psi + s_\psi s_\theta s_\phi & -s_\phi c_\psi + s_\psi s_\theta c_\phi \\ -s_\theta & s_\phi c_\theta & c_\phi c_\theta \end{bmatrix}, \quad (1)$$

$$\mathbf{T} = \begin{bmatrix} 1 & s_\phi t_\theta & c_\phi t_\theta \\ 0 & c_\phi & -s_\phi \\ 0 & s_\phi / c_\theta & c_\phi / c_\theta \end{bmatrix}. \quad (2)$$

To prevent singularity, the Euler angles are bounded with $\theta, \phi \in (-\pi/2, \pi/2)$ and $\psi \in (-\pi, \pi)$ while $c_j = \cos(j), s_j = \sin(j), t_j = \tan(j)$ with $j = [\phi, \theta, \psi]$ and $\mathbf{R}$ is an orthogonal matrix, so $\mathbf{R}^{-1} = \mathbf{R}^T$ hold. In this paper, the following assumption is considered [5].

Assumption 1. *Since the ϕ, θ would not have large deflection, we can consider $T \approx I_3$ than $\omega_B \approx \dot{\Phi}$.*

With the aforementioned kinematic modeling, the dynamic model of each aerial manipulator with account for the interactive force resulting from the movement of the manipulator and slung load motion is described as

$$\begin{aligned} m\ddot{\zeta} &= RF\mu_3 - m_{uav}g\mu_3 + F_{mani} + F_{Load}, \\ J\dot{\omega}_B &= \tau_i - \omega_B \times J\omega_B + \tau_{mani} + \tau_{Load}, \end{aligned} \quad (3)$$

where m denotes the mass of the entire aerial manipulator and half of the load mass, m_{uav} denotes the mass of the quadrotor, including the quadrotor and manipulator, F is the design thrust input to the quadrotor, τ is the thrust moment torque to the quadrotor, g is the gravity constant, $\mu_3 = [0,0,1]^T$, and $J = diag[I_x, I_y, I_z] \in \mathbb{R}^{3\times3}$ denotes the inertia matrix of the quadrotor. Additionally, $F_{mani} \in \mathbb{R}^3$ and $\tau_{mani} \in \mathbb{R}^3$ denote the interactive force/torque from the manipulator, and $F_{Load} \in \mathbb{R}^3$ and $\tau_{Load} \in \mathbb{R}^3$are the interactive force/torque from the load to the quadrotor along the corresponding axes.

Under Assumption 1, the decoupled quadrotor dynamic equation can be expressed as [19]

$$\begin{aligned}
\ddot{x} &= (c_\psi s_\theta c_\phi + s_\psi s_\phi)\frac{F}{m} + \frac{F_{mani,x}}{m} + \frac{F_{Load,x}}{m},\\
\ddot{y} &= (-s_\phi c_\psi + s_\psi s_\theta c_\phi)\frac{F}{m} + \frac{F_{mani,y}}{m} + \frac{F_{Load,y}}{m},\\
\ddot{z} &= -\frac{m_{uav}g}{m} + (c_\phi c_\theta)\frac{F}{m} + \frac{F_{mani,z}}{m} + \frac{F_{Load,z}}{m},\\
\ddot{\phi} &= \frac{I_y - I_z}{I_x}\dot{\theta}\dot{\psi} + \frac{\tau_x}{I_x} + \frac{\tau_{mani,x}}{I_x} + \frac{\tau_{Load,x}}{I_x},\\
\ddot{\theta} &= \frac{I_z - I_x}{I_y}\dot{\phi}\dot{\psi} + \frac{\tau_y}{I_y} + \frac{\tau_{mani,y}}{I_y} + \frac{\tau_{Load,y}}{I_y},\\
\ddot{\psi} &= \frac{I_x - I_y}{I_z}\dot{\phi}\dot{\theta} + \frac{\tau_z}{I_z} + \frac{\tau_{mani,z}}{I_z} + \frac{\tau_{Load,z}}{I_z}.
\end{aligned} \tag{4}$$

After addressing the decoupled quadrotor dynamic model, the dynamic model for the manipulator mounted on the base of the quadrotor can be expressed by the Euler–Lagrange equations as

$$M(\eta)\ddot{\eta} + C(\eta,\dot{\eta})\dot{\eta} + G(\eta) = \tau_\eta + J_m^T T_L, \tag{5}$$

where $M(\eta) \in \mathbb{R}^{3\times3}$ is the inertia matrix, $C(\eta,\dot{\eta}) \in \mathbb{R}^{3\times3}$ represents the Coriolis matrix, and $G(\eta) \in \mathbb{R}^3$ denotes the vector of gravitational force, $\tau_\eta = [\tau_{\eta1}, \tau_{\eta2}, \tau_{\eta3}]^T \in \mathbb{R}^3$ is the control input for each joint, $J_m \in \mathbb{R}^{6\times3}$ is the Jacobian matrix of the end-effector on each aerial manipulator, $T_L \in \mathbb{R}^3$ is the external force acting on the end-effector of the manipulator. In this research, the interactive force from the motion of the quadrotor to the manipulator has been neglected due to the values being infinitesimal. Therefore, we focus on the effect of the slung load on the manipulator, and the value for F_{Load} is obtained from the analyses in the next section.

III. Dual Aerial Manipulator with Load Transformation

The main objective of this paper is to assign a time-varying desired trajectory for the slung load to follow; the motion control of the aerial manipulators is implemented to guarantee the load-tracking mission via cooperative transportation. Before addressing the proposed null-space-based controller in Section IV, the analyses of load trajectory and force are addressed in this section.

A. Desired End-Effector Trajectory Transformation

The trajectory of the load transportation includes the position of the mass center and the attitude. The load position is denoted by $q_L = \{X_{L,c}, Y_{L,c}, Z_{L,c}\}$, and the attitude is given as α_L and β_L, which are the orientation of the load on the x-y plane and the x-z plane, respectively. These notations are illustrated in Fig. 2. Where Fig. 2 represent the load witch carried by the two aerial manipulator in Fig. 1. Since the definition for the load attitude keeps the redundancy of the system, the desired end-effector position is considered to be perpendicular to the x-y plane with respect to the world frame Σ_W. The desired trajectory for the load is $q_{Ld} = [x_{Ld}, y_{Ld}, z_{Ld}, \alpha_{Ld}, \beta_{Ld}]$. Next, we can get the desired end-effector trajectory for each aerial manipulator. It is noted that the subscript $i = \{1,2\}$ is added to denote the number of aerial manipulators in the transportation system. First, we define the length of the load as L_L, the length of the cable connects the load and the manipulator end-effector of each agent define as $L_{str,i}$. By using the attitude definition previously, we can obtain the transformation from the desired load trajectory to the desired end-effector trajectory, $\zeta_{me,id} \in \mathbb{R}^3$ with $i = 1,2$, as follow

$$\begin{aligned}
(\zeta_{me,1d})_x &= x_{Ld} - L_L cos(\beta_{Ld})cos(\alpha_{Ld})/2,\\
(\zeta_{me,1d})_y &= y_{Ld} - L_L cos(\beta_{Ld})sin(\alpha_{Ld})/2,\\
(\zeta_{me,1d})_z &= z_{Ld} - (L_L sin(\beta_{Ld}))/2 + L_{str,1},\\
(\zeta_{me,2d})_x &= x_{Ld} + L_L cos(\beta_{Ld})cos(\alpha_{Ld})/2,\\
(\zeta_{me,2d})_y &= y_{Ld} + L_L cos(\beta_{Ld})sin(\alpha_{Ld})/2,\\
(\zeta_{me,2d})_z &= z_{Ld} + (L_L sin(\beta_{Ld}))/2 + L_{str,2}.
\end{aligned} \tag{6}$$

Since it is difficult to keep the cable perpendicular to the x-y plane in Σ_W, the transformation needs to be adjusted accordingly. Therefore, we define the distance between two end-effectors as $EE_{dis} = ||\zeta_{me,1} - \zeta_{me,2}||$ and assume that the mass of the load acting on the two end-effectors is identical. Thus, the relationship between the two end-effectors to the load can be expressed as

$$\begin{aligned}
x_{L,1} &= \frac{(\zeta_{me,1})_x + (\zeta_{me,2})_x}{2} - \frac{(L_L)_{xy}}{2}\cos\theta_R,\\
y_{L,1} &= \frac{(\zeta_{me,1})_y + (\zeta_{me,2})_y}{2} - \frac{(L_L)_{xy}}{2}\sin\theta_R,\\
z_{L,1} &= (\zeta_{me,1})_z - L_{str,1}\sin\Big(\cos^{-1}\Big(\frac{EE_{dis} - L_L}{2L_{str,1}}\Big)\Big),
\end{aligned} \tag{7}$$

$$\begin{aligned}
x_{L,2} &= \frac{(\zeta_{me,1})_x + (\zeta_{me,2})_x}{2} + \frac{(L_L)_{xy}}{2}\cos\theta_R,\\
y_{L,2} &= \frac{(\zeta_{me,1})_y + (\zeta_{me,2})_y}{2} + \frac{(L_L)_{xy}}{2}\sin\theta_R,\\
z_{L,2} &= (\zeta_{me,2})_z - L_{str,2}\sin\Big(\cos^{-1}\Big(\frac{EE_{dis} - L_L}{2L_{str,2}}\Big)\Big),
\end{aligned} \tag{8}$$

where $(L_L)_{xy}/2$ is the distance from the center of the load to the cable-attached position in Fig. 2, θ_R is the rotation angle from Σ_{Lc} to $\Sigma_W$in z axis, $[x_{Li}, y_{Li}, z_{Li}]$ is the load position which attaches the cable to aerial manipulator in Σ_W.

$$\begin{aligned}
(L_L)_{xy} &= \sqrt{L_L^2 - (z_{L,1} - z_{L,2})^2},\\
\theta_R &= \tan^{-1}\Big(\frac{(\zeta_{me,1})_y - (\zeta_{me,2})_y}{(\zeta_{me,1})_x - (\zeta_{me,2})_x}\Big).
\end{aligned} \tag{9}$$

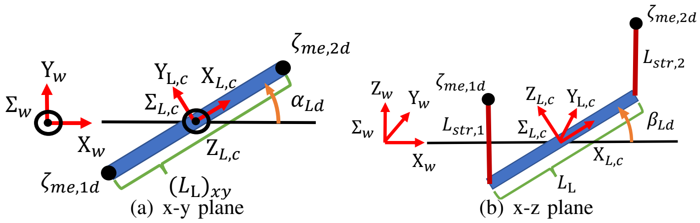

Fig. 2: Sketch and coordinates of the slung load.

Consequently, the position of the load center can be obtained from $[x_{Li}, y_{Li}, z_{Li}]$ that $x_L = (x_{L,1} + x_{L,2})/2$, $y_L = (y_{L,1} + y_{L,2})/2$, and $z_L = (z_{L,1} + z_{L,2})/2$.

B. Cable Tension and Interactive Force

After we get the geometric relationship between the end-effector and load, the cable tension and interactive force can be obtained subsequently. In this research, we only consider the gravity effect on the load and assume that the mass acting on each aerial manipulator is the same. Thus, the tension on each cable to the slung load can be described as

$$\begin{aligned} \vec{P}_{L,i} &= \zeta_{me,i} - [x_{L,i}, y_{L,i}, z_{L,i}]^T, \\ \tan(\theta_{str,i}) &= \frac{(P_{L,i})_z}{\sqrt{(P_{L,i})_x^2 + (P_{L,i})_y^2}}, \\ T_{L,i} &= \frac{m_L g P_{L,i}}{2sin(\theta_{str,i})||P_{L,i}||}, \end{aligned} \tag{10}$$

where m_L is the mass of the load, $P_{L,i} \in \mathbb{R}^3$ is the vector from the end-effector to the load attach point in each agent, $\theta_{str,i}$ is the angle of the cable in Σ_{Lc}, $T_{L,i} \in \mathbb{R}^3$ is the tension force from load to the end-effector in Σ_W.

$$\begin{aligned} F_{Load,i} &\approx R_i T_{L,i}, \\ \tau_{Load,i} &\approx R_i((\zeta_i - \zeta_{me,i}) \times T_{L,i}). \end{aligned} \tag{11}$$

By assuming that the inertia matrix of the manipulator is smaller than quadrotors, the influence of the manipulator motion to the quadrotor can be simplified and given as [7]

$$\begin{aligned} F_{mani,i} \approx & -m_i R_i(\omega_{B,i} \times (\omega_{B,i} \times r_{oc,i}) + \dot{\omega}_{B,i} \times r_{oc,i} \\ & + 2\omega_{B,i} \times \dot{r}_{oc,i} + \ddot{r}_{oc,i}) - m_{mani,i} g, \\ \tau_{mani,i} \approx & \, m_i \Big(r_{oc,i} \times R_i^{-1}(g e_3 - \ddot{\zeta}_i) \Big) - \frac{m_i^2}{m_{mani,i}} r_{oc,i} \times \ddot{r}_{oc,i} \\ & - \frac{m_i^2}{m_{mani,i}} \omega_{B,i} \times (r_{oc,i} \times \dot{r}_{oc,i}), \end{aligned} \tag{12}$$

where $m_{mani,i}$ is the total mass of the manipulator in the i-th agent, $r_{oc,i} \in \mathbb{R}^3$ is the vector from the quadrotor to the center mass of the aerial manipulator system.

IV. Controller Design and Stability Analysis

The control structure of the dual aerial manipulator transportation system with a slung load is shown in Fig. 3. The second UAV use the same strategy. It is composed of four parts, including the desired trajectory calculator, NSB controller, adaptive controller UAV, and adaptive controller for the manipulator.Since the cooperative transportation system is accomplished by using null-space-based control, the main task is to ensure the trajectory tracking of the slung load to the desired trajectory (6). With the given of the load desired trajectory $q_{Ld} = [x_{Ld}, y_{Ld}, z_{Ld}, \alpha_{Ld}, \beta_{Ld}]$ under the assumption of perpendicular cable to the x-y plan, the desired trajectory for the end-effector of the aerial manipulator can be obtained accordingly as $\zeta_{me,id} \in \mathbb{R}^3 \quad i = 1, 2$. These trajectories will be utilized in this section to design the controller.

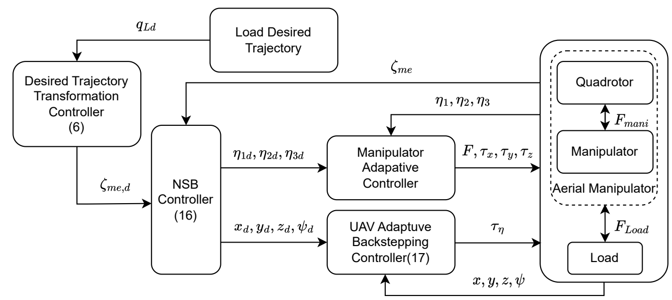

Fig. 3: Framework for aerial manipulator system.

A. NSB Control

The desired trajectory calculator is used to transform the desired trajectory from the load mass center to the end-effector of each aerial manipulator. The NSB controller is used to transform the end-effector trajectory to the desired value of each state. The subtask of the system is also considered in this part, including UAV obstacle avoidance, manipulator joint angle limitation, and other purposes [20]–[22].

In this research, we assume the task of end-effector tracking the main task by changing the desired end-effector trajectory to the desired generalized coordinates. Moreover, we consider the subtask in the NSB controller, such as the UAV obstacle avoidance. The main goal is to keep the tracking performance on the end-effector and subtask at the same time. Thus, the main task can be described as

$$\dot{\zeta}_{me,i} = J(\Phi_i, \Phi_{e,i}, \eta)\dot{q}_i, \tag{13}$$

where $\Phi_i \in \mathbb{R}^3$ is the UAV Euler angle as defined previously, $\Phi_{e,i} \in \mathbb{R}^3$ is the end-effector Euler angle, and $J \in \mathbb{R}^{3\times 9}$ is the Jacobian matrix from the end-effector to the generalized coordinate [22]. Since the quadrotor system is an underactuated system, i.e., only four independent control inputs are available against the six degrees of freedom, the redundancy in the null space can be further utilized. In this research, we choose the position of UAV $\zeta_i = [x_i, y_i, z_i]^T$ and the yaw angle ψ_i as the controlled variables, while row angle ϕ_i and pitch angle θ_i is used as the intermediate control inputs in the proposed controller. Then we can define the control variable as

$$q_{i,c} = [x_i, y_i, z_i, \psi_i, \eta_i]^T, \quad q_{i,u} = [\phi_i, \theta_i]^T \tag{14}$$

so (13) can be rewritten as

$$\dot{\zeta}_{me,i} = J_c \dot{q}_{i,c} + J_u \dot{q}_{i,u}, \tag{15}$$

where $J_c \in \mathbb{R}^{3\times7}$ is the controllable Jacobian matrix, $J_u \in \mathbb{R}^{3\times2}$ is the uncontrolled Jacobian matrix, which is separate from the Jacobian matrix J from the controlled variables. Next, (15) is utilized to design the main task of the NSB controller, and the controller is designed as

$$\begin{aligned}\dot{q}_{i,cd} &= J_c^{\dagger}(\dot{\zeta}_{me,id} + \Lambda_{NSB}\widetilde{\zeta}_{me,i} - J_u\dot{q}_{i,ud}) \\ &\approx J_c^{\dagger}(\dot{\zeta}_{me,id} + \Lambda_{NSB}\widetilde{\zeta}_{me,i}),\end{aligned} \tag{16}$$

where $J_c^{\dagger} = J_c^T(J_cJ_c^T)^{-1}$ is the right pseudo-inverse of J_c, Λ_{NSB} is the positive constant gain, $\widetilde{\zeta}_{me,i} = \zeta_{me,id} - \zeta_{me,i}$ is the position error for the end-effector. Since we consider the roll and pitch change at a small angle, we ignore the effect of the roll and pitch. One of the advantages of NSB control is the design of secondary tasks in the null space. In this paper, the subtasks are considered so that when the aerial manipulators during cooperative transportation on ensuring the tracking of the slung load, the position of the quadrotor can be utilized to enhance system performance. Due to page restrictions, further information on the subtask design can be found in [21]. Compare NSB controller with other control strategy, this method can consider the priority of each task. This make the system more flexible and adjustable than other controller.

B. Adaptive Backstepping Control

The adaptive controller is used to control the UAV to the desired trajectory from the NSB controller with the model uncertainties, disturbance, and interactive forces from the load and manipulator. The adaptive controller for the manipulator is used to control the manipulator to track the desired joint angles calculate from the NSB controller with the effect of the load. The quadrotor system is divided into four subsystems for the design backstopping structure to make each state the virtual input. Designing each of the adaptive laws in the controller by using the Lyapunov stability analysis. First, we define the state of the UAV system as $X = [x, y, z, \phi, \theta, \psi, \dot{x}, \dot{y}, \dot{z}, \dot{\phi}, \dot{\theta}, \dot{\psi}]$. Defining the control inputs as

$$\begin{aligned}&R_fF = \hat{m}\bar{F} - [\hat{F}_{xd}, \hat{F}_{yd}, \hat{F}_{zd}]^T, \quad F = ||R_fF||, \\ &\tau_x = \hat{I}_x\bar{\tau}_x - \hat{\tau}_{xd}, \quad \tau_y = \hat{I}_y\bar{\tau}_y - \hat{\tau}_{yd}, \quad \tau_z = \hat{I}_z\bar{\tau}_z - \hat{\tau}_{zd}.\end{aligned} \tag{17}$$

By denoting c as a positive gain, γ is the renewal rate for the adaptive parameters. $R_f = R\mu_3$, $e_1 = \zeta - \zeta_d$, $\dot{e}_1 = e_2 - c_1e_1$, $e_2 = \dot{\zeta} - \dot{\zeta}_d - c_1e_1$, $e_3 = \phi - \phi_d$, $\dot{e}_3 = e_4 - c_3e_3$, $e_4 = \dot{\phi} - \dot{\phi}_d - c_3e_3$, $e_5 = \theta - \theta_d$, $\dot{e}_5 = e_6 - c_5e_5$, $e_6 = \dot{\theta} - \dot{\theta}_d - c_5e_5$, $e_7 = \psi - \psi_d$, $\dot{e}_7 = e_8 - c_7e_7$, $e_8 = \dot{\psi} - \dot{\psi}_d - c_7e_7$, $\Phi_\phi = \dot{\theta}\dot{\psi}$, $\Phi_\theta = \dot{\phi}\dot{\psi}$, $\Phi_\psi = \dot{\phi}\dot{\theta}$. $\Theta_\phi = (I_y - I_z)/I_x$, $\Theta_\theta = (I_z - I_x)/I_y$, $\Theta_\psi = (I_x - I_y)/I_z$. The nominal control inputs are given as

$$\begin{aligned}\bar{F} &= -e_1 - c_2e_2 + g\mu_3 + \ddot{\eta}_d - c_1\dot{e}_1 \\ \bar{\tau}_x &= -e_3 - c_4e_4 + \ddot{\phi}_d - c_3\dot{e}_3 - \hat{\Theta}_\phi\Phi_\phi \\ \bar{\tau}_y &= -e_5 - c_6e_6 + \ddot{\theta}_d - c_5\dot{e}_5 - \hat{\Theta}_\theta\Phi_\theta \\ \bar{\tau}_z &= -e_7 - c_8e_8 + \ddot{\psi}_d - c_7\dot{e}_7 - \hat{\Theta}_\psi\Phi_\psi\end{aligned} \tag{18}$$

For the system stability we can get the adaptive law $\hat{m}, \hat{I}_x, \hat{I}_y, \hat{I}_z, \hat{\Theta}_\phi, \hat{\Theta}_\theta, \hat{\Theta}_\psi$ for the controller to renew the estimate parameters given as [19]

$$\begin{aligned}&\dot{\hat{m}} = -\gamma_m e_2^T\bar{F}, \ \dot{\hat{I}}_x = -\gamma_x e_4\bar{\tau}_x, \ \dot{\hat{I}}_y = -\gamma_y e_6\bar{\tau}_y, \\ &\dot{\hat{I}}_z = -\gamma_z e_8\bar{\tau}_z, \ \dot{\hat{\Theta}}_x = \gamma_\phi e_4\Phi_\phi, \ \dot{\hat{\Theta}}_y = \gamma_\theta e_6\Phi_\theta, \\ &\dot{\hat{\Theta}}_z = \gamma_\psi e_8\Phi_\psi.\end{aligned} \tag{19}$$

Next, we design the control input to solve the interactive forces from the manipulator and the load. We consider the disturbance to be bounded and changes at a small rate in the interactive force and torque in Σ_W, and assume the update rate can handle the change, then the control input for the disturbance is designed as

$$\begin{aligned}&\dot{\hat{F}}_{xd} = \gamma_{xd}e_2^T\mu_1, \ \dot{\hat{F}}_{yd} = \gamma_{yd}e_2^T\mu_2, \ \dot{\hat{F}}_{zd} = \gamma_{zd}e_2^T\mu_3, \\ &\dot{\hat{\tau}}_{xd} = \gamma_{\phi d}e_4, \ \dot{\hat{\tau}}_{yd} = \gamma_{\theta d}e_6, \ \dot{\hat{\tau}}_{zd} = \gamma_{\psi d}e_8,\end{aligned} \tag{20}$$

where $\mu_1 = [1, 0, 0]^T, \mu_2 = [0, 1, 0]^T, \mu_3 = [0, 0, 1]^T$. The presented adaptive algorithms are utilized to control the quadrotor under the framework of the proposed decoupling approach. The control input may change to the rotating speed of each rotor in [1]. The adaptive controller for the manipulator is used in this research.

C. Stability Analysis

The stability and convergence of the tracking errors for quadrotors under the effect of the coupling force from the manipulator, load, and model uncertainties are addressed in this section. The dynamics of the quadrotor with the coupling effect from the manipulator and load are presented in (4). We choose the positive-definite Lyapunov function candidate as

$$\begin{aligned}V = \frac{1}{2}\Big(&\sum_{n=1}^{2} e_i^Te_i + \sum_{n=3}^{8} e_i^2 + \frac{\widetilde{m}^2}{\gamma_m m} + \frac{\widetilde{I}_x^2}{\gamma_x I_x} + \frac{\widetilde{I}_y^2}{\gamma_y I_y} \\ &+ \frac{\widetilde{I}_z^2}{\gamma_z I_z} + \frac{\widetilde{\Theta}_\phi^2}{\gamma_\phi} + \frac{\widetilde{\Theta}_\theta^2}{\gamma_\theta} + \frac{\widetilde{\Theta}_\psi^2}{\gamma_\psi} + \frac{\widetilde{F}_{dis}^2}{\gamma_{dis}m} + \frac{\widetilde{\tau}_{xd}^2}{\gamma_{\phi d}I_x} \\ &+ \frac{\widetilde{\tau}_{yd}^2}{\gamma_{\theta d}I_y} + \frac{\widetilde{\tau}_{zd}^2}{\gamma_{\psi d}I_z}\Big),\end{aligned} \tag{21}$$

where $\widetilde{m} = m - \hat{m}$, $\widetilde{I}_a = I_a - \hat{I}_a$ for $a = [x, y, z]$, $\widetilde{\Theta}_b = \Theta_b - \hat{\Theta}_b$ for $b = [\phi, \theta, \psi]$ are the estimation errors of the enclosed signals, $\gamma_{dis} = diag\{\gamma_{xd}, \gamma_{yd}, \gamma_{zd}\}$, $F_{dis} = F_{mani} + F_{Load}$ is the sum of the interactive forces of the load and manipulator, and $\widetilde{F}_{dis}$ is the error of the estimation disturbance. By taking the time derivative of V along the trajectory of the closed-loop control system, we get [5], [19]

$$\dot{V} = -\sum_{n=1}^{2} c_ie_i^Te_i - \sum_{n=3}^{8} c_ie_i^2 \leq 0. \tag{22}$$

The adaptive control laws presented in the previous section are utilized in the derivative of $\dot{V}$ with referring to [5], [19]. Since V is positive-definite and $\dot{V} \leq 0$ is a non-increasing function, all the states are asymptotically stable, with the assumption of the interaction force change slowly and close to zero.

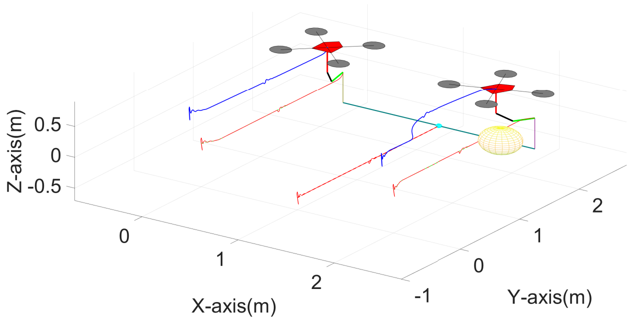

Fig. 4: 3-D tracking of the load and the quadrotor position left(UAV1), and the right(UAV2).

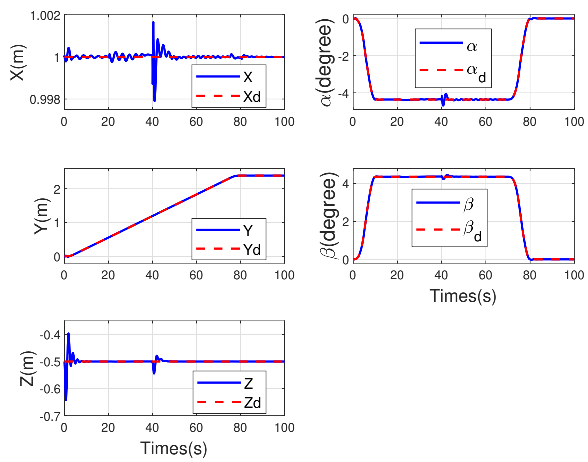

Fig. 5: Position trajectory of the slung load in the system.

V. Simulation Results

The simulations of the proposed control structure of the dual aerial manipulator transportation with cable are conducted in this section. The simulation gives the load's desired trajectory and considers the obstacle in the environment. The obstacle is located at $\{2.5, 1, 0.5\}$. In the load trajectory, we also change the load attitude. The main goal is for the quadrotor to avoid obstacles and keep the load-tracking performance. The load trajectory $x_{L,d}, y_{L,d}, z_{L,d}, \alpha_{L,d}, \beta_{L,d}$ is designed in second order differentiable shows in Fig. 5. The parameters of the aerial manipulator are designed the same given as TABLE I. Next, we add change $m_L = 0.2(kg)$ when $t = 40s$, the result are shown in Figs. 4 to 7. In Fig. 4 shows the tracking in 3-D with the obstacle, here shows the UAV obstacle avoidance subtask, the distance between obstacle and UAV shows in Fig. 7. We can see that the tracking performance of load in Fig. 7. The tracking for UAV and manipulator in Fig. 8,Fig. 9. Two aerial manipulators use different desired value to keep the load tracking. The error at 40s comes from the change of load mass. The proposed controller may estimate the unknown parameter to keep load tracking in Fig. 6. All the unknown parameters are stable, and the UAV2's unknown parameters are also stable.The result shows that our proposed controller

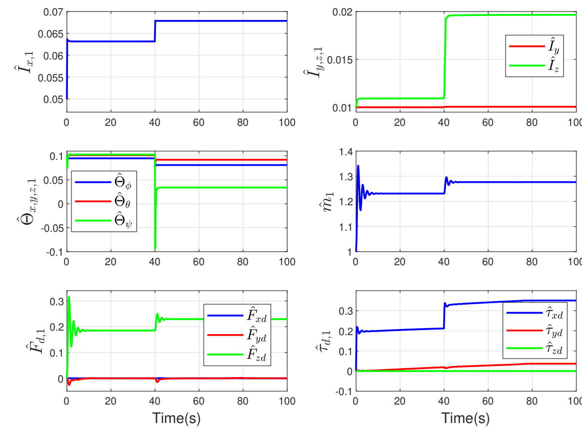

Fig. 6: UAV1 estimation of the unknown parameters and interactive forces.

can handle the interactive force and the change of the load mass in the tracking.

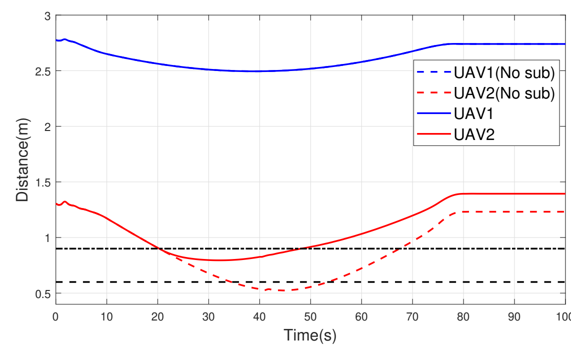

Fig. 7: Distance between UAVs to the obstacle.

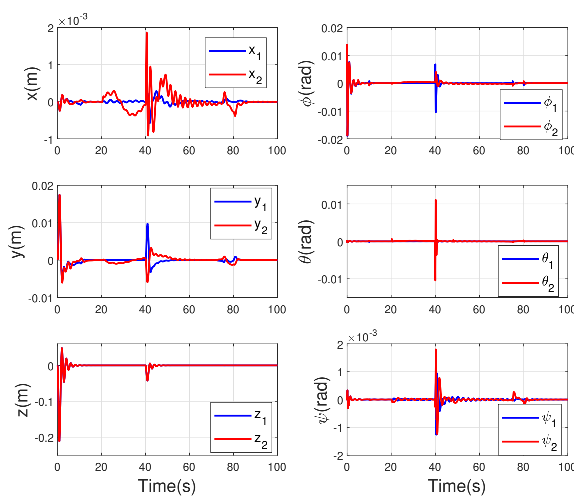

Fig. 8: Tracking error of two UAVs.

VI. Conclusion

In this paper, the cooperative aerial transportation control strategy is proposed. The proposed controller uses the load as the leader, given a desired trajectory, then the two

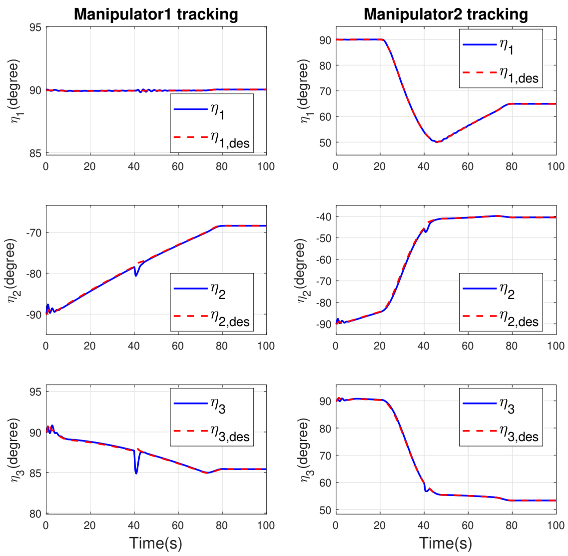

Fig. 9: Position trajectory tracking of the manipulator.

aerial manipulators can keep the tracking performance with the model uncertainties, interactive force, and the obstacle avoidance subtask. With the cable added, the system can handle the larger disturbance. Next, the load position is not needed, we use the position of each aerial manipulator to get the load position. This is closer to the real situation. The Lyapunov theorem is utilized to show system stability, and tracking performance is guaranteed for the proposed system. A numerical example is presented to show the efficiency of the proposed control system. In future work, experiments with the proposed controller will be done along with the design strategies for UAV subtask collision avoidance. In the experiment, the position and attitude of UAV may use motion capture and the joint angle of manipulator may catch from the motor encoder.

TABLE I: Parameters

UAV	$I_x = I_y = 3.2 \times 10^{-3}(kg - m^2)$ $I_z = 5 \times 10^{-3}(kg - m^2), m_{uav} = 0.9(kg)$
Manipulator	$m_{mani,1,2,3} = [0.1; 0.1; 0.1](kg)$ $L_{mani,1,2,3} = [0.4; 0.2; 0.2](m)$ $I_{mani,x,y,z} = 0.03(kg - m^2)$
Load	$m_L = 0.1(kg), L_L = 2(m), L_{str,i} = 0.5(m)$
Control Parameters	$c_1 = c_2 = diag\{1, 1, 1\}, c_3 = c_4 = 5$ $c_5 = c_6 = 10, c_7 = c_8 = 1$ $K_p = 1, K_d = 1, K_\eta = diag\{1, 1, 1\}$ $\Lambda_{NSB} = [1, 1, 1], R = 0.9(m), r = 0.6(m)$
Adaptive Rate	$\gamma_m = 0.1, \gamma_x = 0.5, \gamma_y = 1, \gamma_z = 100$ $\gamma_{\phi_1} = 10^5, \gamma_{\phi_2} = 10^3, \gamma_{\theta_1} = 10^5$ $\gamma_{\theta_2} = 10^3, \gamma_{\psi_1} = 10^6, \gamma_{\psi_2} = 10^4$ $\gamma_{xd,yd,zd} = 1, \gamma_{\phi d,\theta d} = 10, \gamma_{\psi d} = 1$

References

[1] T.-W. Ou and Y.-C. Liu, "Adaptive backstepping tracking control for quadrotor aerial robots subject to uncertain dynamics," in *2019 American Control Conference (ACC)*. IEEE, 2019, pp. 1–6.

[2] X. Lin, Y. Yu, and C.-Y. Sun, "A decoupling control for quadrotor uav using dynamic surface control and sliding mode disturbance observer," *Nonlinear Dynamics*, vol. 97, no. 1, pp. 781–795, 2019.

[3] S. Liu, B. Niu, G. Zong, X. Zhao, and N. Xu, "Data-driven-based event-triggered optimal control of unknown nonlinear systems with input constraints," *Nonlinear Dynamics*, vol. 109, no. 2, pp. 891–909, 2022.

[4] S. A. Emami and A. Banazadeh, "Simultaneous trajectory tracking and aerial manipulation using a multi-stage model predictive control," *Aerospace Science and Technology*, vol. 112, p. 106573, 2021.

[5] Y.-C. Liu and C.-Y. Huang, "Ddpg-based adaptive robust tracking control for aerial manipulators with decoupling approach," *IEEE Transactions on Cybernetics*, vol. 52, no. 8, pp. 8258–8271, 2022.

[6] A. Jimenez-Cano, J. Braga, G. Heredia, and A. Ollero, "Aerial manipulator for structure inspection by contact from the underside," in *2015 IEEE/RSJ International Conference on Intelligent Robots and Systems (IROS)*. IEEE, 2015, pp. 1879–1884.

[7] G. Zhang, Y. He, B. Dai, F. Gu, J. Han, and G. Liu, "Robust control of an aerial manipulator based on a variable inertia parameters model," *IEEE Transactions on Industrial Electronics*, vol. 67, no. 11, pp. 9515–9525, 2019.

[8] J. E. Sierra and M. Santos, "Wind and payload disturbance rejection control based on adaptive neural estimators: application on quadrotors," *Complexity*, vol. 2019, 2019.

[9] G. Muscio, F. Pierri, M. A. Trujillo, E. Cataldi, G. Giglio, G. Antonelli, F. Caccavale, A. Viguria, S. Chiaverini, and A. Ollero, "Experiments on coordinated motion of aerial robotic manipulators," in *2016 IEEE International Conference on Robotics and Automation (ICRA)*. IEEE, 2016, pp. 1224–1229.

[10] Y. Alothman, W. Jasim, and D. Gu, "Quad-rotor lifting-transporting cable-suspended payloads control," in *2015 21st International Conference on Automation and Computing (ICAC)*. IEEE, 2015, pp. 1–6.

[11] Z. A. Ali and H. Zhangang, "Maneuvering control of hexrotor uav equipped with a cable-driven gripper," *IEEE Access*, vol. 9, pp. 65 308–65 318, 2021.

[12] A. Hegde and D. Ghose, "Multi-uav collaborative transportation of payloads with obstacle avoidance," *IEEE Control Systems Letters*, vol. 6, pp. 926–931, 2021.

[13] G. Li, R. Ge, and G. Loianno, "Cooperative transportation of cable suspended payloads with mavs using monocular vision and inertial sensing," *IEEE Robotics and Automation Letters*, vol. 6, no. 3, pp. 5316–5323, 2021.

[14] H. Lee, H. Kim, and H. J. Kim, "Planning and control for collision-free cooperative aerial transportation," *IEEE Transactions on Automation Science and Engineering*, vol. 15, no. 1, pp. 189–201, 2016.

[15] G. Gioioso, A. Franchi, G. Salvietti, S. Scheggi, and D. Prattichizzo, "The flying hand: A formation of uavs for cooperative aerial tele-manipulation," in *2014 IEEE International Conference on Robotics and Automation (ICRA)*. IEEE, 2014, pp. 4335–4341.

[16] F. Caccavale, G. Giglio, G. Muscio, and F. Pierri, "Cooperative impedance control for multiple uavs with a robotic arm," in *2015 IEEE/RSJ International Conference on Intelligent Robots and Systems (IROS)*. IEEE, 2015, pp. 2366–2371.

[17] T. Chen and J. Shan, "Cooperative transportation of cable-suspended slender payload using two quadrotors," in *2019 IEEE International Conference on Unmanned Systems (ICUS)*. IEEE, 2019, pp. 432–437.

[18] H. Xie, K. Dong, and P. Chirarattananon, "Cooperative transport of a suspended payload via two aerial robots with inertial sensing," *IEEE Access*, vol. 10, pp. 81 764–81 776, 2022.

[19] Y.-C. Liu and T.-W. Ou, "Nonlinear adaptive tracking control for quadrotor aerial robots under uncertain dynamics," *IET Control Theory and Application*, vol. 15, no. 8, pp. 1126–1139, 2021.

[20] G. Antonelli, F. Arrichiello, and S. Chiaverini, "The null-space-based behavioral control for autonomous robotic systems," *Intelligent Service Robotics*, vol. 1, no. 1, pp. 27–39, 2008.

[21] Y.-C. Liu and N. Chopra, "Control of semi-autonomous teleoperation system with time delays," *Automatica*, vol. 49, no. 6, pp. 1553–1565, 2013.

[22] K. Baizid, G. Giglio, F. Pierri, M. A. Trujillo, G. Antonelli, F. Caccavale, A. Viguria, S. Chiaverini, and A. Ollero, "Experiments on behavioral coordinated control of an unmanned aerial vehicle manipulator system," in *2015 IEEE International Conference on Robotics and Automation (ICRA)*. IEEE, 2015, pp. 4680–4685.